Supplementary Information (SI) for Journal of Materials Chemistry A.

Supporting Information

Photo-thermo-electric conversion system based on photothermal organic cocrystal composite film for outdoor self-power supply

Rui Wei,[a] Changxiang Shao,*[a] Xiaoqing Liu,[a] Huijun Kong,[a] Weiyan Li,[b] Jiahui Yu,[a] Baolei Wang,[a] Chuanying Wang,[a] Bingyu Pan,[a] Bingpeng Guo,*[c] Zhongqian Song,*[b]

[a.] School of Chemistry and Pharmaceutical Engineering, Medical Science and Technology Innovation Center, Shandong First Medical University and Shandong Academy of Medical Sciences, Jinan, 250117, P. R. China.

Email: cxshao@sdfmu.edu.cn

[b.] College of Medical Information and Artificial Intelligence, Shandong First Medical University and Shandong Academy of Medical Sciences, Jinan, 250117, P. R. China.

Email: zqsong@sdfmu.edu.cn

[c.] Shandong Provincial Key Laboratory of Molecular Engineering, School of Chemistry and Chemical Engineering, Qilu University of Technology (Shandong Academy of Sciences), Jinan, 250103, P. R. China.

Email: guobingpeng@qlu.edu.cn

Supplementary Figures

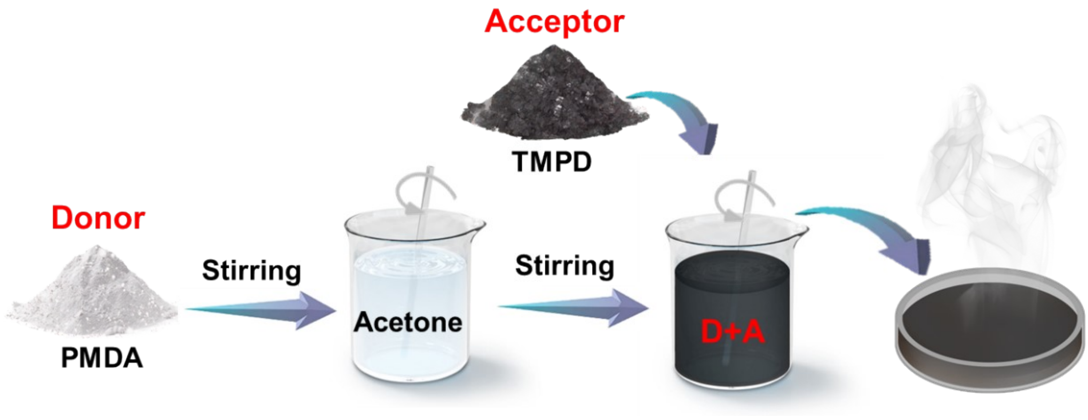

Fig. S1. Schematic illustration of the preparation of TMPD-PMDA.

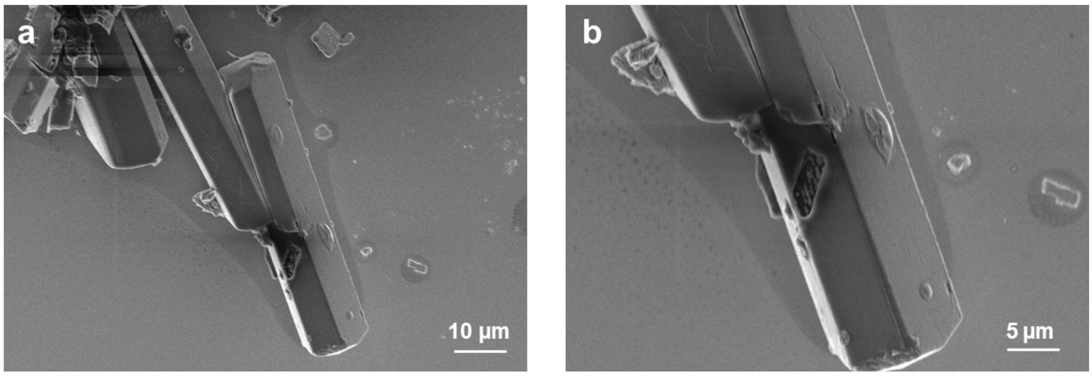

Fig. S2. (a,b) SEM images of TMPD-PMDA at different magnifications.

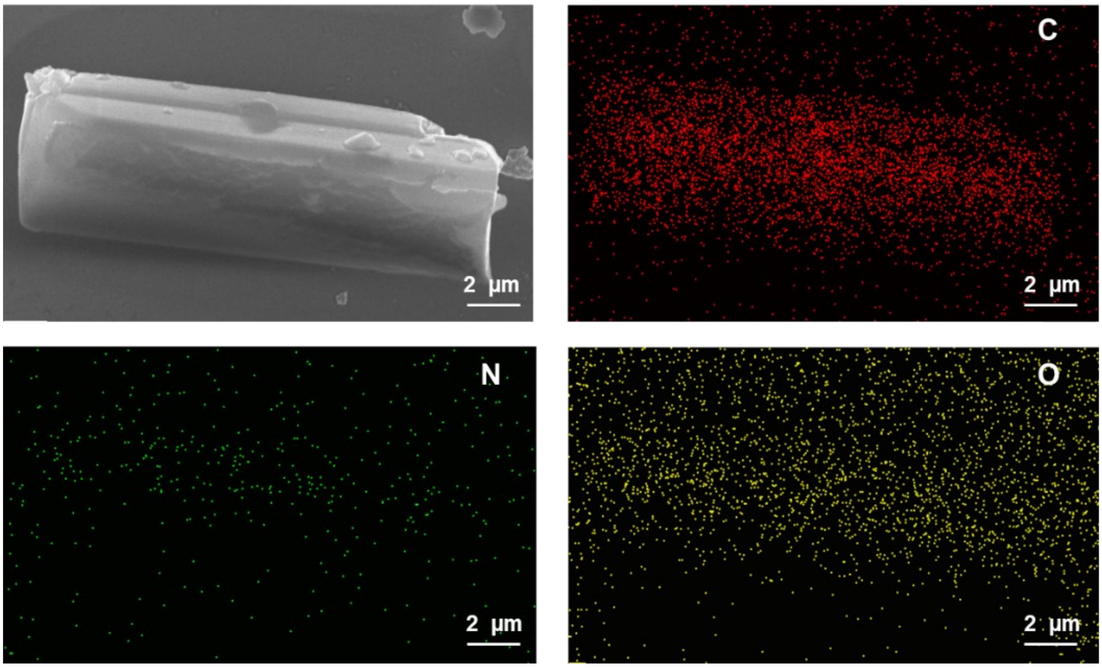

Fig. S3. SEM image of TMPD-PMDA and the corresponding EDS mapping images, showing the distribution of C, N, and O elements.

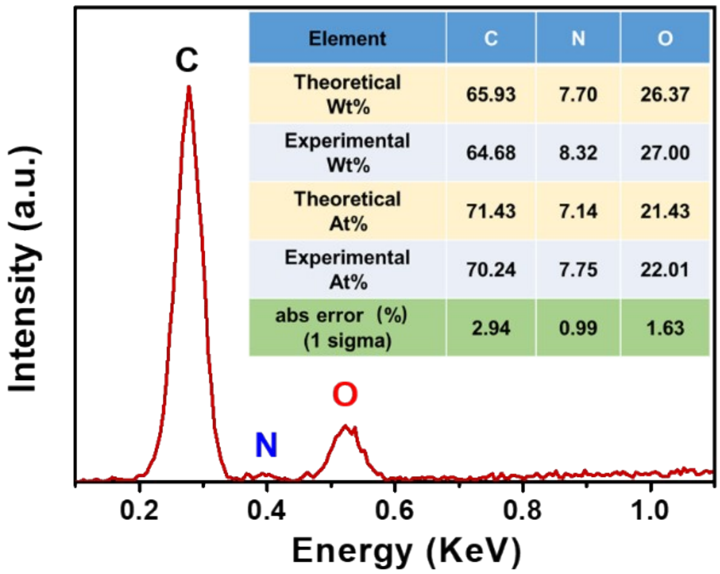

Element	C	N	O
Theoretical Wt%	65.93	7.70	26.37
Experimental Wt%	64.68	8.32	27.00
Theoretical At%	71.43	7.14	21.43
Experimental At%	70.24	7.75	22.01
abs error (%) (1 sigma)	2.94	0.99	1.63

Fig. S4. EDS spectrum and elemental composition of TMPD-PMDA cocrystal.

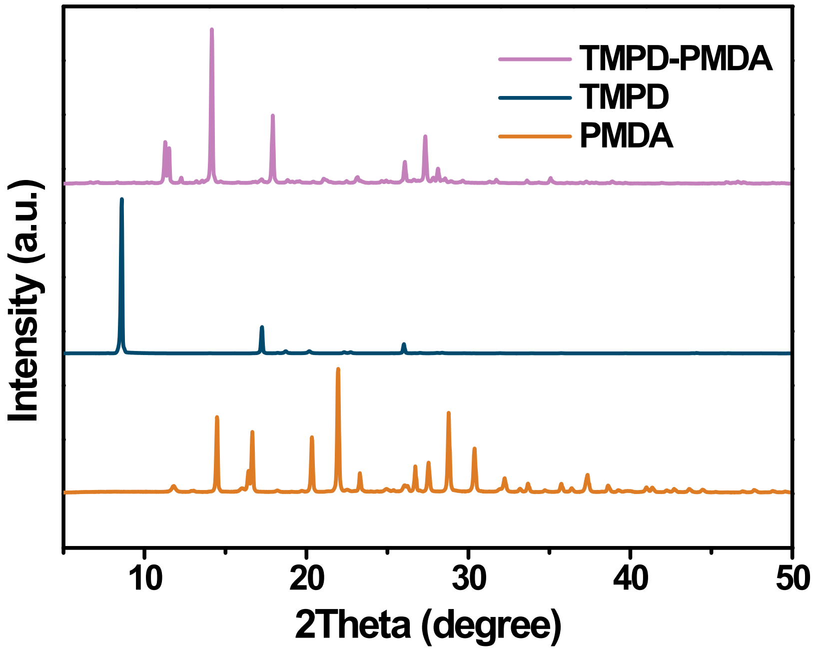

Fig. S5. XRD patterns of TMPD, PMDA and TMPD-PMDA powder.

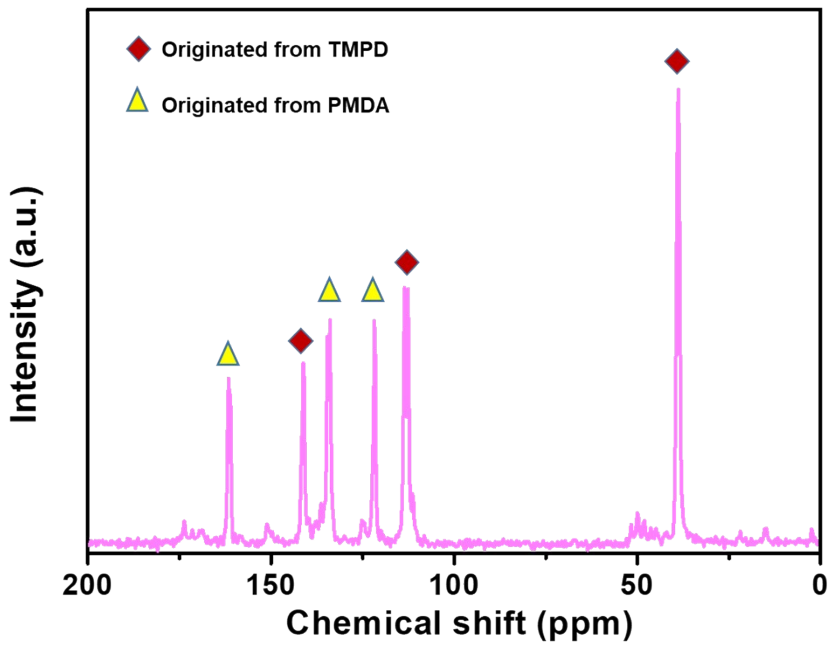

Fig. S6. Solid-state ^{13}C NMR spectra of TMPD-PMDA cocrystal.

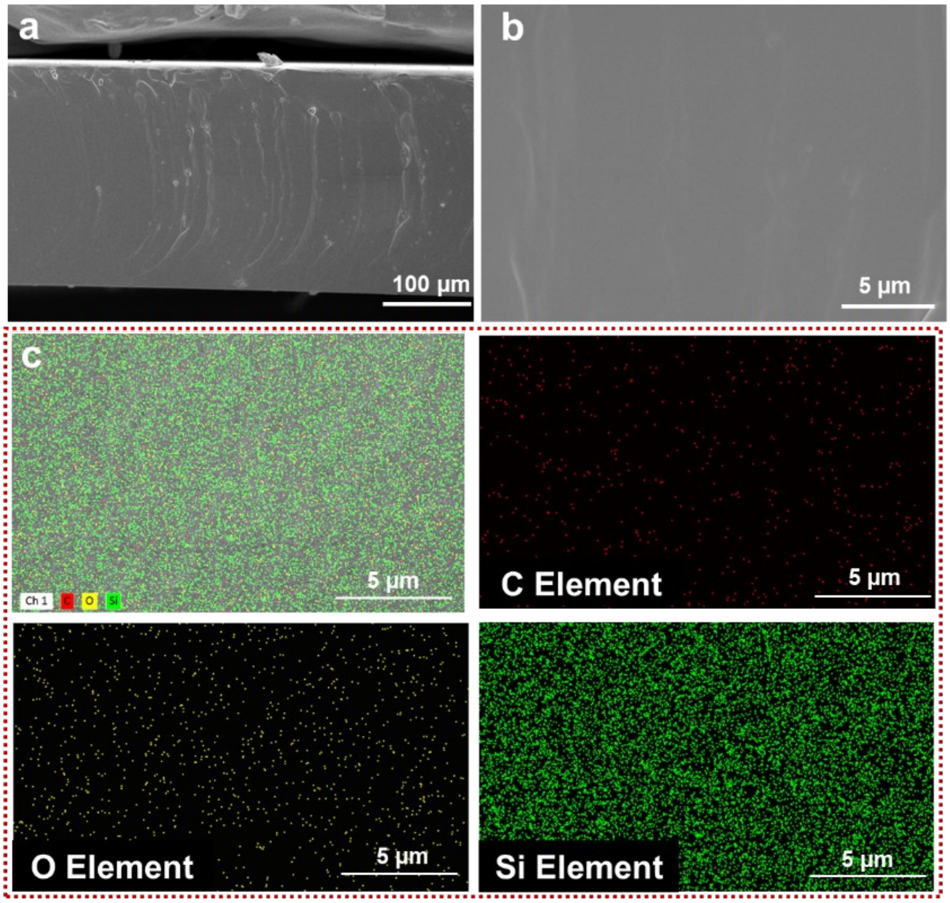

Fig. S7. (a,b) SEM images of the pure PDMS film at different magnifications, revealing a smooth surface. (c) EDS mapping images of the PDMS film, showing the distribution of C, O, and Si elements.

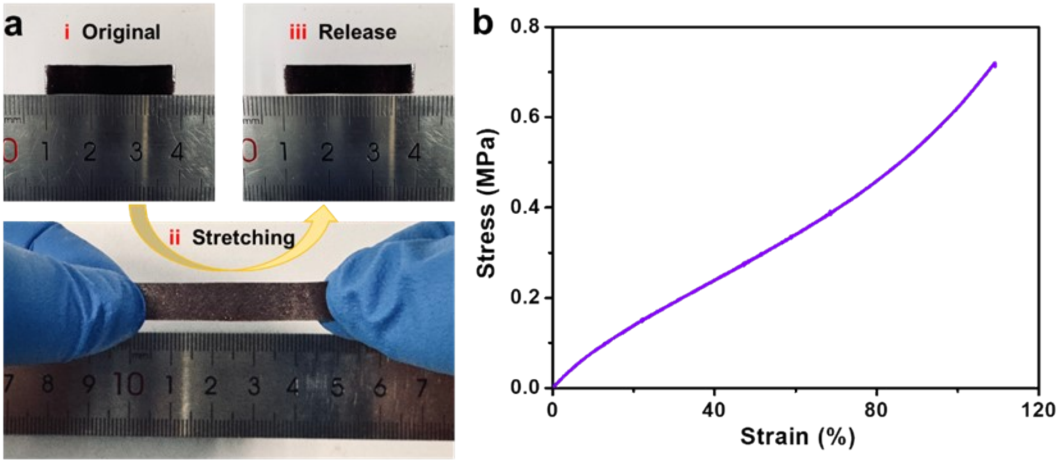

Fig. S8. Stretchability of the TPF. (a) Photographs of the TPF film (i) in its initial state, (ii) under stretching, and (iii) after release. (b) The stress-strain curve of TPF.

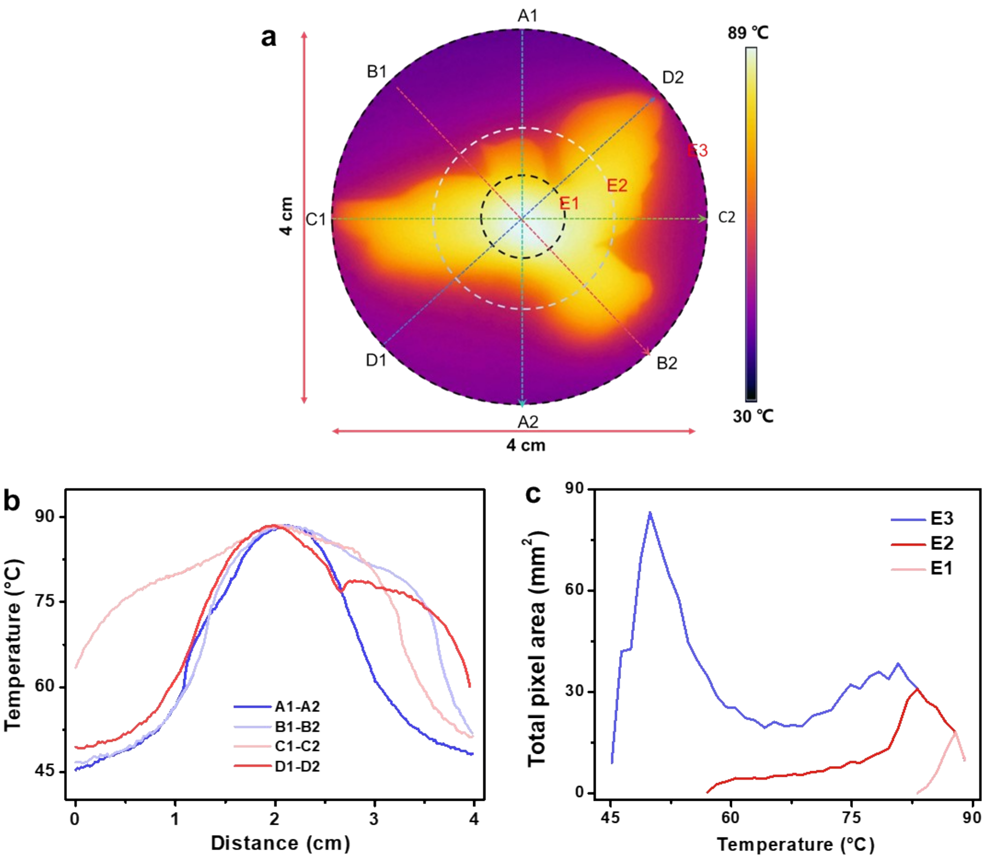

Fig. S9. (a) IR images of the bird shaped TPF. (b) Temperature distribution along A1-A2, B1-B2, C1-C2, D1-D2. (c) The total pixel area corresponding to each temperature within the E1, E2 and E3 regions.

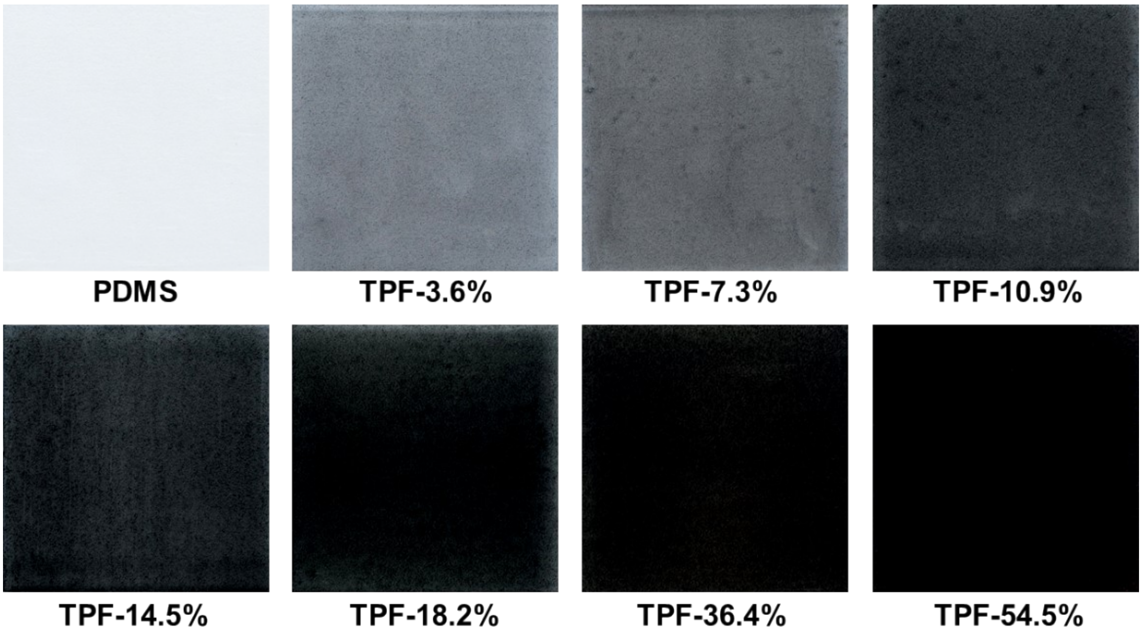

Fig. S10. Images of PDMS films with varying TFP content, ranging from 3.6% to 54.5%, showing the visual appearance of the films as the TFP concentration increases.

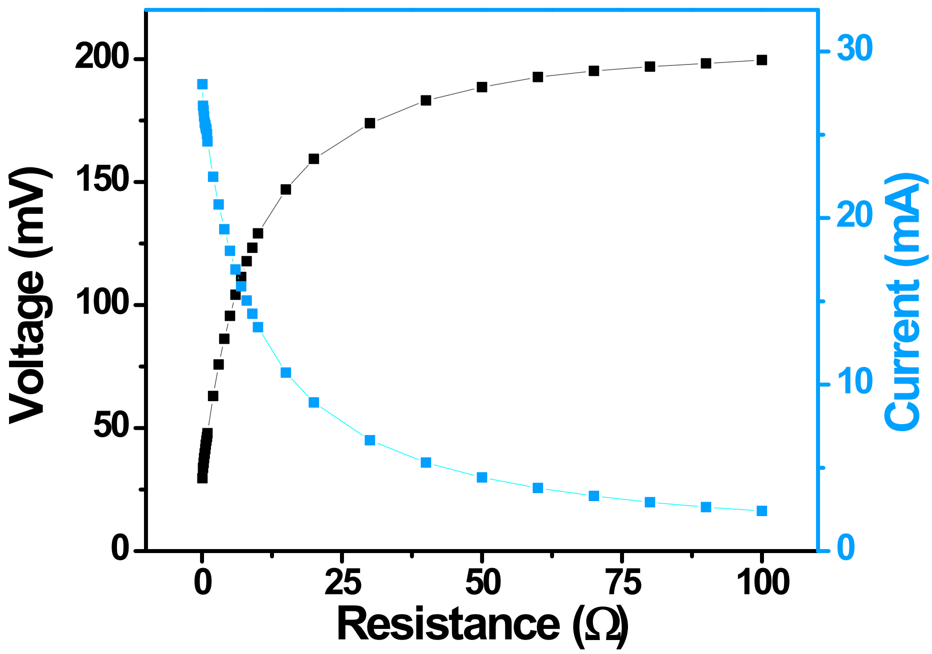

Fig. S11. Dependence of potential and current on load resistance of the external circuit.

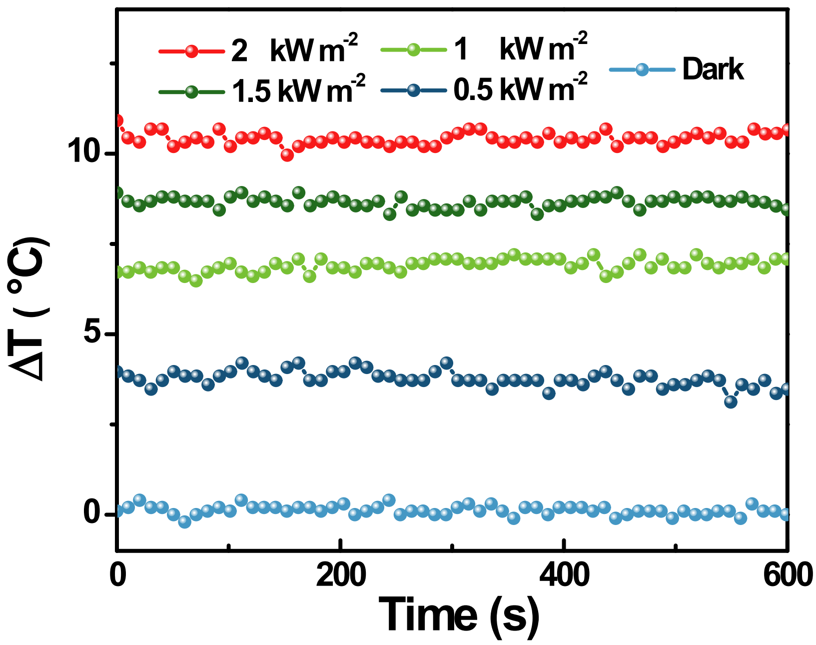

Fig. S12. The temperature difference of between the hot and cold ends of the TEG under different power densities over time.

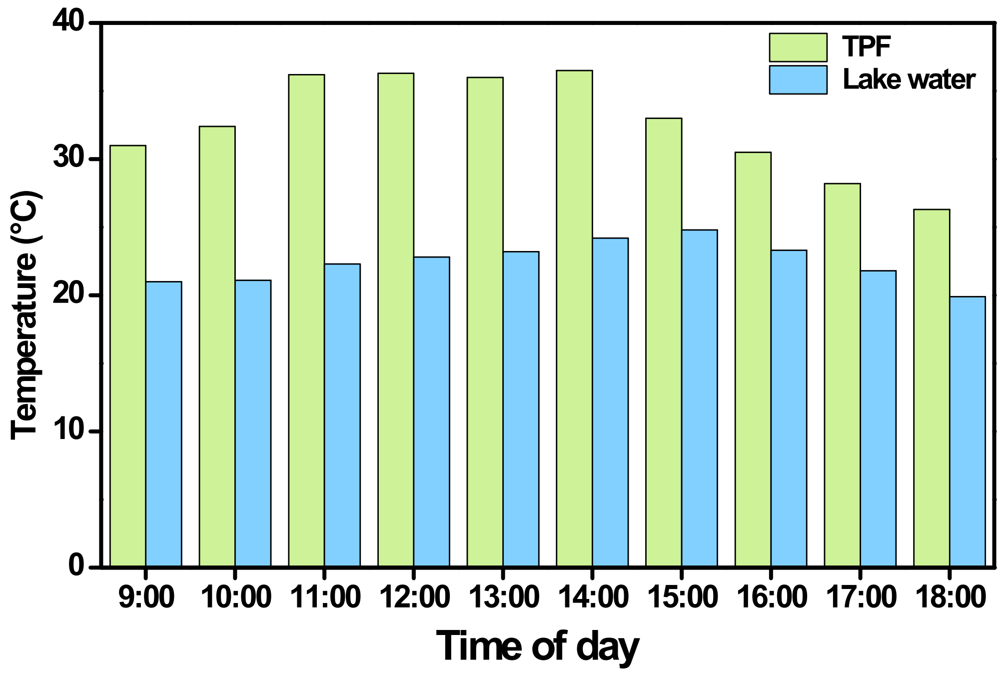

Fig. S13. Temperature variation of the TPF surface and lake water outdoor at different times throughout the day.

Table S1. Comparison of representative photothermal organic materials/ cocrystals and their performance in solar-thermal-electric conversion.

Photothermal materials		Maximum temperature (1 sun)	Photo-thermal-electric conversion system			Power generation performance (1sun)				References
			Photothermal layer	TEG model (size)	Refrigeration device	Temperature difference	V_{oc} (mV)	I_{sc} (mA)	P_{max} (W m^{-2})	
Organic small molecule	CR-DPA-T	110 °C (808 nm laser, 0.8 W cm^{-2})	H-PDMS/CR-DPA-T film	Self-made TEG (43×40 mm^2)	environment	8.9	42	~15	0.09	Adv. Mater. 2022, 34, 2108048
	GDPA-QCN	56 °C	GDPA-QCN powder	TEC1-12706 (40×40×3.6 mm^3)	Circulating cooling water	2~3	90~100	-	-	Angew. Chem. Int. Ed. 2022, 61, 14, e202117087
	DDPA-PDN	146 °C (655 nm laser, 0.8 W cm^{-2})	DDPA-PDN mixed thermal conductive adhesive	TEC1-12706 (40×40×3.6 mm^3)	Circulating cooling water	2~3	83	-	-	Adv. Funct. Mater. 2021, 31, 49, 2106247
	4OCSPC	50 °C	4OCSPC powder	TEC1-12706 (40×40×3.6 mm^3)	Circulating cooling water	4.6	124	-	-	J. Mater. Chem. A. 2021, 9, 24452-24459
	DCN4CQA	45 °C	DCN4CQA@Paper	TEC1-12706	Circulating cooling water	~4.3	91.52	-	0.3625	Chem. Eur. J. 2022, 28, 20, e202104137
	TPA-SBTQ	62 °C	TPA-SBTQ mixed thermal conductiv	TEC1-12706	Circulating cooling water	~4	106	-	-	*Adv. Funct. Mater.* **2024**, 34, 25, 2315762

			e adhesive							
	2TP-BBT	57 °C	2TP-BBT mixed thermal conductive silicone grease	TEC1-12706	Circulating cooling water	3.8	95.5	-	-	J. Mater. Chem. A, 2023, 11, 15380-15388
	GTPA-BTO-Py+	~70 °C	GTPA-BTO-Py+	TEC1-12706 (40×40×3.6 mm^3)	Circulating cooling water	~5	~140	-	-	Chem. Eng. J., 2023, 471, 144745
	DDHT	55 °C	DDHT mixed thermal conductive silicone grease	TEC1-12706	Circulating cooling water	6.1	90.3	-	-	ACS Appl. Energy Mater. 2022, 5, 15758-15767
	TPyP	128 °C (730 nm laser, 0.8 W cm^{-2})	TPyP powder	TEC1-12706	Circulating cooling water	4.3	104	-	-	RSC Adv., 2022, 12, 28997
	BQC	61 °C	BQC mixed thermal grease	TEC1-12706	Circulating cooling water	5.9	112.8	-	-	Angew. Chem. Int. Ed. 2024, 63, e202402726
	NOMe-D	47 °C	NOMe-D mixed conductive adhesive	TEC1-335-5.5-6	Circulating cooling water	-	241	-	-	Adv. Mater. 2025, 37, e11877
	TTC	55.1 (808 nm laser, 0.116 W cm^{-2})	TTC-PU photothermal membrane	Self-made CNT based TEG	Simulated skin	-	32.8 V m^{-2}		196×10^{-6}	Science Advances 2023，9, 50, eadh8917
cocrystal	CBC	46 °C	CBC mixed resin	TEG 1-127-3.6-3	Heat sink		130~143	25	-	Natl. Sci. Rev., 2025, 12, 5, nwaf121
	TQC	61 °C (808 nm laser, 0.5 W cm^{-2})	TQC and a thermally conductiv	TEC1-12701 (40×40×5.2	Circulating cooling water		427	22.6	2.21	ACS Energy Lett. 2023, 8, 4179-4185

				mm^3)						
			e double-sided adhesive	TEC1-12706 (40×40×3.6 mm^3)		7.6	122.8	~17	1.31	
	TMPD-PMDA	77 °C	TPF	SP1848-27145 SA (40×40×3.6 mm^3)	Circulating cooling water	6.9	195	33.5	1.11	This work